



HAL
open science

Proterozoic magmatic events recorded in $^{40}\text{Ar}/^{39}\text{Ar}$ data from the northern part of the Kedougou Kenieba Inlier (eastern Senegal)

I. Sagna, X. Quidelleur, E. Dioh, P. Y. Gillot, J. C. Lefèvre, Lenka Baratoux,
D. P. Diallo

► To cite this version:

I. Sagna, X. Quidelleur, E. Dioh, P. Y. Gillot, J. C. Lefèvre, et al.. Proterozoic magmatic events recorded in $^{40}\text{Ar}/^{39}\text{Ar}$ data from the northern part of the Kedougou Kenieba Inlier (eastern Senegal). *Journal of African Earth Sciences*, 2021, 175, 10.1016/j.jafrearsci.2021.104109 . insu-03661473

HAL Id: insu-03661473

<https://insu.hal.science/insu-03661473>

Submitted on 13 Feb 2023

HAL is a multi-disciplinary open access archive for the deposit and dissemination of scientific research documents, whether they are published or not. The documents may come from teaching and research institutions in France or abroad, or from public or private research centers.

L'archive ouverte pluridisciplinaire **HAL**, est destinée au dépôt et à la diffusion de documents scientifiques de niveau recherche, publiés ou non, émanant des établissements d'enseignement et de recherche français ou étrangers, des laboratoires publics ou privés.



Distributed under a Creative Commons Attribution - NonCommercial 4.0 International License

1 **Proterozoic magmatic events recorded in $^{40}\text{Ar}/^{39}\text{Ar}$ data from the northern**
2 **part of the Kedougou Kenieba Inlier (eastern Senegal)**

3
4 I. Sagna^a, X. Quidelleur^{b,*}, E. Dioh^a, P.Y. Gillot^b, J.C. Lefèvre^c, L. Baratoux^{a,d} and D.P.
5 Diallo^f

6
7 ^a Institut Fondamental d’Afrique Noire Cheikh Anta Diop, BP 206, Université Cheikh Anta Diop, Dakar,
8 Sénégal

9 ^b Université Paris-Saclay, CNRS, GEOPS, Orsay, 91405, France

10 ^c ARAR, UMR5138, CDRC, Villeurbanne, F-69622; France

11 ^d Laboratoire GET, Université Toulouse 3 Paul Sabatier, IRD, CNRS UMR 5563, Observatoire Midi-Pyrénées,
12 31400 Toulouse, France

13 ^fDépartement de Géologie, Faculté des Sciences et Techniques, Université Cheikh Anta Diop, Dakar, Senegal

14 *: corresponding author

15

16

17 **Keywords:** $^{40}\text{Ar}/^{39}\text{Ar}$ thermochronology; Proterozoic; West African Craton; Senegal;
18 Kedougou Kenieba Inlier

19

20

21 Content: Abstract: 206 words

22 Text: 3843 words

23

24 Figure 1: Map of studied area

25 Figure 2a: Hornblende and biotite Ar/Ar age spectra

26 Figure 2b: K-Feldspar Ar/Ar age spectra

27 Figure 3: Thermal history and modelled K-Feldspar age spectra

28

29 Table 1: Ar/Ar ages

30

31 Supp. Mat.: Ar/Ar data

32 Supp. Mat. 2: Monotonic cooling modelling of K-Feldspar age spectra

33

34

35

36

37 Rev3 version – November 19th, 2020

38

39
40
41
42
43
44
45
46
47
48
49
50
51
52
53
54
55
56
57
58

ABSTRACT

We present a thermal history of the Kedougou Kenieba Inlier (eastern Senegal), the western-central outcropping part of the West African Craton, based on $^{40}\text{Ar}/^{39}\text{Ar}$ analyses performed on hornblende, biotite, and K-feldspar minerals from Paleoproterozoic plutonic rocks. $^{40}\text{Ar}/^{39}\text{Ar}$ age spectra obtained for hornblendes and biotites range between 2055 ± 26 and 2028 ± 28 Ma, in very good consistency. They suggest that magmatism in the Kedougou Kenieba Inlier happened at the end of the Eburnean Orogeny (2.25-2.00 Ga). Taking into account previous zircon U/Pb ages, these new results imply that initial cooling from magmatic temperature to about 300°C (biotite closure temperature) occurred rapidly, and that these rocks did not experience any subsequent re-heating event above 300°C. On the other hand, $^{40}\text{Ar}/^{39}\text{Ar}$ age spectra obtained on K-feldspars display strongly disturbed patterns revealing that these minerals experienced argon loss due to re-heating events. Altogether, these data constrain a thermal history for the studied area involving two thermal events with temperatures around 275 and 225°C, at about 1750 and 1500 Ma, respectively. These thermal events, previously inferred from U/Pb ages of intruding mafic dykes, can be related to aborted attempts of continental breakup, as the West African Craton remained attached to Baltica and Amazonia cratons during the 1.8-1.3 Ga interval.

59 **1. Introduction**

60
61 Proterozoic plate reconstruction models (e.g., Johansson 2009; Zhao *et al.*, 2002)
62 suggest that the West African craton (WAC), the north-east of Central South America
63 (Amazonia) craton, and the south-east of East European (Baltica) craton were connected for
64 more than 1 Ga, until breakup of Rodinia (c.a. 0.8 Ga; Johansson, 2009; 2014; Wingate and
65 Giddings, 2000).

66 The Eburnean Orogeny completed the assemblage of the WAC at ca. 2.1 Ga (Baratoux
67 *et al.*, 2011; Begg *et al.*, 2009; Feybesse *et al.*, 2006; Wane *et al.*, 2018, and references
68 therein). The Trans-Amazonian Orogeny in South America led to the assembly of the
69 Amazonian Craton at ca. 2.18-1.95 Ga (Kroonenberg *et al.*, 2016; Nomade *et al.*, 2002;
70 Hartmann, 2002; Neves *et al.*, 2006). The WAC was then separated from the Baltica at about
71 600-550 Ma (Johansson, 2009; 2014), and from the Amazonia craton at about 200 Ma, when
72 the Central Atlantic Ocean opened (e.g., Marzoli *et al.*, 1999; Nomade *et al.*, 2007; Merle *et al.*,
73 2011). The Mesoproterozoic period was considered as relatively quiet for the WAC, as no
74 tectonic event was documented. However, recent studies have identified during this period
75 large-scale magmatic events based on U-Pb ages obtained on dyke swarms (Baratoux *et al.*,
76 2019; Youbi *et al.*, 2013).

77 $^{40}\text{Ar}/^{39}\text{Ar}$ analyses have been performed here on hornblende, biotite and K-feldspar
78 minerals from mafic and felsic Paleoproterozoic plutonic rocks intruding the Mako belt in
79 order to reconstruct the thermal history of the Kedougou Kenieba Inlier (WAC). The aim of
80 the present study is also to contribute to the identification of large-scale magmatic events
81 having affected the WAC and to determine their thermal impact using $^{40}\text{Ar}/^{39}\text{Ar}$
82 thermochronology.

83

84 **2. Geological setting**

85

86 *2.1. West African Craton*

87

88 Archean to Paleoproterozoic crusts from the WAC outcrop as the Reguibat Rise and
89 the Leo-Man Rise, in its northern and southern parts, respectively (Fig. 1). Neoproterozoic to
90 Paleozoic rocks from the Taoudeni Basin cover its central part. In the western part of the
91 Reguibat Rise, the main phase of magmatism is dated at about 2.9 Ga (Schofield *et al.*, 2012).
92 Then, metamorphism occurred at 2.7 Ga, as suggested by the age obtained there for granulite

93 facies gneisses (Cahen *et al.*, 1984). In the Man Domain of the Leo Rise, comparable ages
94 have been measured for the Archean formation, but U-Pb ages obtained for gneiss reveal that
95 magmatism started as early as 3.5 Ga (Thiéblemont *et al.*, 2004).

96 The WAC experienced an intense crustal growth between 2.2 and 2.1 Ga (e.g.,
97 Abouchami *et al.*, 1990; Dia *et al.*, 1997; Hirdes and Davis, 2002). It is characterized by
98 emplacement of tonalite-trondhjemite-granodiorite (TTG) series, granite plutons, and
99 intercalated greenstone belts. Based on its tholeiitic or calc-alkaline signature, the latter has
100 been related to a metamorphosed volcanic arc environment (Dia, 1988). During the Eburnean
101 Orogeny, several periods of deformation have been recognized with different interpretations
102 proposed (e.g., Feybesse *et al.*, 2006; Perrouy *et al.*, 2012). First, a compression episode
103 induced regional metamorphism due to thrusting and crustal thickening. Then, possibly
104 following an extension phase, N to NE transcurrent shear zones developed during the second
105 period. Overall, a voluminous plutonic activity occurred during the Eburnean Orogeny in the
106 WAC. Calc-alkaline Na-rich plutonism of TTG-type was first emplaced and was followed by
107 more alkaline syenitic magmatism (Baratoux *et al.*, 2011), from about 2250 to 2060 Ma (e.g.,
108 Goujou *et al.*, 2010; Hirdes and Davis, 2002; Tshibubudze *et al.*, 2013; Wane *et al.*, 2018). At
109 least 26 dyke swarms of variable orientations were mapped across the WAC using the
110 airborne magnetic data (Jessell *et al.*, 2015). These dyke swarms were emplaced between
111 ~2733 Ma (Tait *et al.*, 2013) and ~200 Ma (Baratoux *et al.*, 2019).

112

113 2.2. Kedougou Kenieba Inlier (KKI)

114

115 The Birimian supergroup, mapped in detail by Theveniaut *et al.* (2010), makes up
116 most of the Kedougou Kenieba Inlier (WAC, Eastern Senegal) where the present study is
117 focused (Fig. 1). The western part of the Kedougou Kenieba Inlier is made of
118 Paleoproterozoic volcano-plutonic and volcano-sedimentary rocks (Mako belt) crosscut by
119 plutonic bodies of varying composition, from gabbroic to granitic (Dioh *et al.*, 2006) (Fig.1).
120 They were emplaced in an arc-type setting (Dia *et al.* 1997; Sagna *et al.*, 2017) and accreted
121 during the Eburnean Orogeny (Baratoux *et al.*, 2011; Begg *et al.*, 2009; Feybesse *et al.*,
122 2006).

123 To the west of the KKI, the Mako Supergroup is mainly made of tholeiitic and calc-
124 alkaline lavas interbedded with volcano-detritic sediments, which are folded and have
125 undergone a greenschist facies metamorphism (Bassot 1966; 1987; Dia 1988; Dia *et al.*
126 1997). Between 2158 and 2079 Ma, they were intruded by several plutonic bodies from the

127 Badon-Kakadian Batholith (Dia *et al.* 1997). Amphibolite facies metamorphism of Paleo-
128 Proterozoic metasediments, was documented around the northern edge of the Saraya batholith
129 in the central part of the Kedougou Kenieba Inlier (Ndiaye *et al.*, 1989). Within these
130 metasediments, metamorphic monazites yielded LA-ICP-MS U-Pb ages of 2052 ± 7 and 2048
131 ± 8 Ma, and garnets neoblasts were dated using Sm-Nd at 2049.1 ± 3.1 Ma (Kone *et al.*,
132 2018).

133 The volcano-plutonic area investigated here corresponds to the northern part of the
134 Mako Supergroup. Numerous granitoid bodies are present, as well as metabasites tholeites
135 from the Konkoto and Mako areas. The metasediments and calc-alkaline metavolcanites of
136 the Fouldé and Baniomba series are also found in this area (Dia *et al.*, 1997; Dioh *et al.*, 2006;
137 Goujou *et al.*, 2010; Gueye *et al.*, 2007, and references therein). Granodiorite rocks have been
138 sampled from the Diombalou (981M) and the Kaourou–Alinguel (984M and 9814M) plutons.
139 Sample 983M is from a fine-grained amphibole-bearing rock within the Badon pluton, while
140 9813M is from a lower gabbroic unit from the Sansankhoto pluton (Fig.1). The Badon
141 batholith (981M) was recently dated at 2102 ± 8 Ma (U-Pb, zircon; Théveniaut *et al.*, 2010)
142 and the Sansankhoto batholith (9813M) yields 2058 ± 8 Ma (U-Pb zircon; Goujou *et al.*,
143 2010).

144 Recent K-Ar ages, performed on hornblende, biotite and K-feldspar minerals from the
145 same samples as those investigated in the present study, have shown that plutonism in the
146 Kedougou Kenieba Inlier occurred between 2.0 and 2.1 Ga, and suggested either a slow
147 cooling rate for hundreds of Ma, or that a thermal event partially re-opened the K-Ar system
148 of K-feldspars from this area (Sagna *et al.*, 2017).

149 In the KKI, two dyke swarms were identified using the airborne magnetic data (Jessell
150 *et al.*, 2015): a NNE to NE-trending Kedougou swarm (1764 ± 4 Ma) and an E-W oriented
151 Sambarabougou swarm (1521 ± 3 Ma), both dated by TIMS U-Pb method on baddeleyite
152 grains; Baratoux *et al.*, 2019) (Fig. 1b).

153

154 **3. Methods**

155

156 *3.1. $^{40}\text{Ar}/^{39}\text{Ar}$ dating*

157

158 The $^{40}\text{Ar}/^{39}\text{Ar}$ analyses were performed at Orsay (France) using the multi-collector
159 mass-spectrometer and procedure presented in Coulié *et al.* (2004). During 60 h, samples and
160 flux monitors were irradiated together in the Corvallis Triga reactor (Radiation center, Oregon

161 state University, USA), using the CLICIT facility. Gas extraction of unknowns was realised by
162 step-heating with a high frequency furnace. As their behavior during heating is supposedly
163 ideal, a Nd-YAG laser (1064 nm) was used to fuse 20 mg aliquots of sanidine separated from
164 the Fish Canyon tuff in a single step. From these analyses, the J factors were calculated based
165 on the age of 28.201 Ma (Kuiper *et al.*, 2008). From repeated analyses of air aliquots
166 measured with the same ^{40}Ar signal than that measured for a typical step, the mass
167 discrimination was corrected using a linear law. ^{40}K decay constants and the K isotopic ratio
168 of Steiger and Jäger (1977) have been used.

169 Precise and accurate measurements are mandatory to constrain the age and duration of
170 geological events. We have shown that $^{40}\text{Ar}/^{39}\text{Ar}$ ages with an analytical relative precision as
171 low as 0.1% can be reached with our instrument (Ricci *et al.*, 2013). However, as $^{40}\text{Ar}/^{39}\text{Ar}$ is
172 a relative dating technique, standard ages and decay constant uncertainties are the main
173 limiting factor for the accuracy of this technique (Kuiper *et al.*, 2008). Recent studies have
174 proposed ages for the widely used Fish Canyon Tuff sanidine ranging from 27.89 (Westerhold
175 *et al.*, 2012) to 28.305 ± 0.072 Ma (Renne *et al.*, 2010). Such difference of about 1% can be
176 explained by inter-laboratory biases, or by the presence of previously un-detected $^{39}\text{Ar}_\text{K}$ recoil
177 (Phillips *et al.*, 2017). Consequently, we conservatively use a systematic error of 1% for the J-
178 Factor determination involved in the $^{40}\text{Ar}/^{39}\text{Ar}$ age calculation presented here. Uncertainties
179 are quoted at the 2σ level throughout this manuscript.

180

181 3.1. $^{40}\text{Ar}/^{39}\text{Ar}$ thermochronology

182

183 The multi-diffusion domain (MDD) approach has been used here in order to recover
184 the continuous thermal history recorded in K-feldspars (Lovera *et al.*, 1989; 1992). It relies on
185 the hypothesis that diffusion of Ar occurs in nature by the same mechanics as in the
186 laboratory, and that diffusion of K-feldspar argon can be modeled by a discrete distribution of
187 non-interacting domains. Using the $^{40}\text{Ar}/^{39}\text{Ar}$ step-heating measurements, diffusion
188 parameters (i.e., activation energy and frequency factor) are retrieved from the Arrhenius
189 diagram obtained from the degassing systematics of reactor-produced $^{39}\text{Ar}_\text{K}$ (Lovera *et al.*,
190 1989). Monotonic cooling thermal histories can be obtained through inverse modeling, hence
191 without a-priori thermal history, while forward modeling approach is necessary when re-
192 heating is imposed in the input thermal history.

193

194

195 **4. Results**

196

197 *4.1. $^{40}\text{Ar}/^{39}\text{Ar}$ ages*

198

199 Plateau and integrated $^{40}\text{Ar}/^{39}\text{Ar}$ ages obtained here from the Kedougou Kenieba Inlier
200 are given in Table 1, and full dataset can be found in Supp. Mat. 1. Apparent $^{40}\text{Ar}/^{39}\text{Ar}$ age
201 spectra for hornblendes and biotites yield ages ranging between 2055 ± 26 and 2028 ± 28 Ma,
202 with two clusters at 2033 ± 10 Ma (983M hornblende and 9814M biotite) and 2053 ± 12 Ma
203 (981M hornblende), when considering only the three well-defined plateaus including more
204 than 90% of total ^{39}Ar (Fig. 2). Note that the other 3 plateaus, which include only between 50
205 and 70% of ^{39}Ar , hence satisfying plateau criteria (Fleck et al., 1977), also fall within clusters.
206 Because argon is released in a short temperature interval as dehydration and decomposition of
207 hornblende occur (Wartho *et al.*, 1991), plateau ages are defined here only by few steps.
208 However, they cover a large proportion of the total ^{39}Ar released of 93 and 98%, for 981M
209 and 983M, respectively. Age spectrum for 984M hornblende shows distinct behavior, with
210 increasing ages from about 1800 Ma before reaching a rather poorly defined plateau (58% of
211 total ^{39}Ar) at 2055 ± 26 Ma (Figure 2a). Similarly, 984M and 9813M biotite spectra show
212 slightly disturbed patterns, but yield plateau ages of 2053 ± 26 (66% of total ^{39}Ar) and $2028 \pm$
213 28 Ma (52% of total ^{39}Ar), respectively. Besides younger ages obtained for low temperature
214 steps, 9814M biotite displays a plateau over 93% of ^{39}Ar released with an age of 2034 ± 26
215 Ma (Fig. 2a).

216 K-feldspars age spectra display more disturbed patterns than biotite and amphibole
217 samples (Fig. 2b). Only 981M spectrum can be used to calculate a plateau age of 1793 ± 24
218 Ma between 800 and 1025°C (63% of total ^{39}Ar), although, as it displays overall increasing
219 ages, it should be regarded with caution. However, excluding the first step, apparent ages
220 overall increase from about 1550 to 1900 Ma. The three other feldspar samples do not display
221 any plateau age s.s. and have increasing ages from low to high temperature steps. Sample
222 983M K-feldspar display increasing ages up to 1778 Ma, with a very large step of 1740 Ma
223 obtained between 1175 and 1295°C. Note that it is poorly defined due to the very large
224 amount of gas released. Indeed, it has necessitated the use of the highest measurement range,
225 which lacked a precise calibration. Apparent ages of 984M K-feldspar show a steep increase
226 at low temperature up to about 1500 Ma, followed by a shallower increase of apparent ages
227 up to about 1750 Ma at high temperature. Finally, Sample 9814M K-feldspar displays similar

228 but more pronounced features than the latter, with two pseudo-plateaus at about 1530 Ma
229 between 765 and 945°C, and one at about 1730 Ma for the high temperature steps.

230

231 4.2. $^{40}\text{Ar}/^{39}\text{Ar}$ thermochronology

232

233 Thermal histories from K-feldspars were first retrieved under the assumption of
234 monotonic cooling (Supp. Mat. 2). Note that modeling for 981M K-feldspar was not possible
235 as the age spectrum was obtained from a too low number of temperature steps. For samples
236 984M and 9814M, MDD modeled and measured age spectra match, while for 9814M, they
237 are noticeably different. The three thermal histories obtained here display clear differences,
238 which seems incompatible with a common regional geodynamic history. Furthermore, they
239 suggest cooling through the 300°C isotherm (i.e., the closure temperature of biotite; Hodges,
240 1991) at 1700 Ma for 983M, and at 1400 Ma for 984M and 9814M. This is in strong
241 disagreement with the well-constrained biotite $^{40}\text{Ar}/^{39}\text{Ar}$ ages, ranging from 2028 ± 28 to
242 2053 ± 26 Ma (Fig. 2a and Table 1). Hence, monotonic cooling below 650°C, the closure
243 temperature of hornblende (Harrison and McDougall, 1980), since 2050 Ma cannot account
244 for disturbances observed in K-feldspar $^{40}\text{Ar}/^{39}\text{Ar}$ spectra shown in Fig. 2b. Consequently, it
245 is necessary to invoke one or several re-heating events having affected the study area in order
246 to explain the re-opening of the Ar system recorded in K-feldspars.

247

248 5. Discussion

249

250 5.1. Cooling temperatures of the granitoids

251

252 New $^{40}\text{Ar}/^{39}\text{Ar}$ ages obtained here on hornblendes and biotites range within 2028 ± 14
253 and 2055 ± 10 Ma (Table 1), with a mean age of about 2040 Ma. Comparison with previous
254 K-Ar ages realized on the same samples (Sagna *et al.*, 2017) shows that the $^{40}\text{Ar}/^{39}\text{Ar}$ ages
255 obtained here are more clustered and some are significantly older. This could be explained by
256 the fact that the K-Ar technique is unable to detect loss of radiogenic argon from the less
257 retentive sites during thermal events (e.g., McDougall and Harrison, 1999). On the other
258 hand, such loss seems to have been recorded by the $^{40}\text{Ar}/^{39}\text{Ar}$ technique, as shown by the
259 younger ages obtained here from low temperature steps of biotite and hornblende samples
260 (Fig. 2a). Previously published $^{40}\text{Ar}/^{39}\text{Ar}$ hornblende, biotite and muscovite ages from the
261 whole KKI range between 2212 and 2020 Ma (Gueye *et al.*, 2007), in agreement with the

262 present study. However, as samples come from different units than those investigated here, no
263 direct comparison can be performed.

264 We have calculated cooling rates using a closure temperature of 900°C for zircon U-
265 Pb ages (Lee et al., 1997), 550°C for hornblende $^{40}\text{Ar}/^{39}\text{Ar}$ ages (McDougall and Harrison,
266 1999), and 300°C for biotite $^{40}\text{Ar}/^{39}\text{Ar}$ ages (Hodges, 1991). For the Badon batholith, based on
267 the U-Pb zircon age of 2102 ± 8 Ma (Théveniaut *et al.*, 2010), and the $^{40}\text{Ar}/^{39}\text{Ar}$ hornblende
268 ages of 2053 ± 12 and 2055 ± 10 Ma for 981M and 984M, respectively (Table 1), we have
269 calculated cooling rates of $7^\circ\text{C}.\text{Myr}^{-1}$. An even lower rate of $5^\circ\text{C}.\text{Myr}^{-1}$ is obtained for sample
270 983M, which displays and $^{40}\text{Ar}/^{39}\text{Ar}$ hornblende ages of 2032 ± 12 Ma (Table 1). Within the
271 range 900°C-300°C, cooling rates of about $10^\circ\text{C}.\text{Myr}^{-1}$ are calculated when considering
272 biotite ages of 2053 ± 10 and 2034 ± 8 Ma, for 984M and 9814M samples, respectively
273 (Table 1). A significantly higher rate of $20^\circ\text{C}.\text{Myr}^{-1}$ is obtained when considering only the
274 Sansankhoto pluton dated at 2058 ± 8 Ma with U-Pb on zircon (Goujou *et al.*, 2010), and at
275 2028 ± 28 Ma using $^{40}\text{Ar}/^{39}\text{Ar}$ on biotite (Table 1).

276 Cooling rates of batholiths emplaced within other more recent convergent geodynamic
277 settings show values on the order of those reported above for the KKI batholith from about
278 900 to 300°C (e.g., Maurel et al., 2004; Quidelleur et al., 1997).

279

280 *5.2. Re-opening of the $^{40}\text{Ar}/^{39}\text{Ar}$ system during younger thermal events*

281

282 The flat shape of the biotite age patterns (Fig. 2a) suggest that there was no further
283 thermal event reaching a temperature higher than 300°C after emplacement of the batholith.

284 Regarding K-feldspars, Figure 2b shows that the apparent age spectra of all three
285 samples display disturbed patterns suggesting that they experienced one or several moderate
286 thermal perturbations younger than 1800 Ma. As continuous cooling cannot account for
287 $^{40}\text{Ar}/^{39}\text{Ar}$ age spectra from K-feldspar, we have attempted a modeling of the thermal history
288 including re-heating events. The thermal history used to compute the K-feldspar age spectra
289 using forward MDD modelling (Lovera, 1992) is shown in Figure 3. This thermal history has
290 been constructed using previous zircon U-Pb ages (Goujou *et al.*, 2010; Théveniaut *et al.*,
291 2010), hornblende and biotite ages from this study (Table 1), and their associated closure
292 temperature (see section 5.1). In addition, we have included two 10 Ma long re-heating events
293 at 1750 and 1500 Ma, of 275 and 225°C, respectively, suggested by the K-feldspar $^{40}\text{Ar}/^{39}\text{Ar}$
294 spectra described in the results section. Using this input thermal history, all modelled age

295 spectra display $^{40}\text{Ar}/^{39}\text{Ar}$ age spectra that are rather similar to measured spectra (Fig. 3
296 inserts).

297 In the KKI, two dyke swarms were dated using TIMS U-Pb on baddeleyites (Baratoux
298 et al, 2019): a NE oriented Kedougou dyke swarm at 1764 ± 4 Ma, and an E-W oriented
299 Sambarabougou swarm at 1521 ± 3 Ma (Baratoux *et al.*, 2019). The two dated swarms occur
300 in the study area, even though not in the immediate vicinity of the granitoids studied here. The
301 closest NE oriented dyke is located ca 10 km far north from the granitoids while the E-W
302 dykes are even farther, about 50 km to the north. There is also a possibility that the dykes are
303 closer to the study area, but they are too small or too deep to be mapped by airborne magnetic
304 data. In any case, the two ages at ca 1750 and 1500 Ma, inferred from K-feldspars age
305 spectra, are similar to the ages obtained by U-Pb method on the two dyke swarms (Baratoux
306 et al., 2019) and, therefore, we suggest that reopening of the $^{40}\text{Ar}/^{39}\text{Ar}$ system may be related
307 to these two regional thermal events.

308

309 5.3. Chronology of the thermal events in the WAC

310

311 Regional dyke swarms are often considered as the arrival of a mantle plume at the
312 base of the lithosphere (e.g., Park et al., 1995; Li et al., 1999; Ernst, 2014), or emplaced from
313 a shallow mantle source related to lithospheric extension (e.g., Jourdan et al., 2007; Hastie
314 et al., 2014; Merle *et al.*, 2014). In both cases, such intrusion of regional dyke swarms can
315 induce large-scale thermal effects.

316 Within the WAC, the Libiri and Kedougou thermal events, dated at 1790 and 1750
317 Ma, respectively (Baratoux *et al.*, 2019), and the 1750 Ma Tagragra of Akka event (Youbi *et*
318 *al.*, 2013) have been identified based on the U-Pb ages of dyke swarms. As these dykes are
319 converging towards the northeast of the WAC (Baratoux *et al.*, 2019), it can be assumed that
320 this area was the locus of an intense magmatic activity which is manifested by several pulses
321 around 1750 Ma. Youbi *et al.* (2013) suggest that the mafic dykes and felsic dykes of four
322 Anti-Atlas Inliers are derived from a 1.75 Ga bimodal felsic-mafic magmatism emplaced in a
323 continental rifting setting. All together, these ages can be interpreted as the occurrence of two
324 thermal events (Baratoux *et al.*, 2019). The first one at 1790 Ma, from the west to the center
325 of the Amazonia, Libiri in WAC, and some of the Sarmatia dykes in Baltica. The second one
326 at 1765 Ma, from the youngest swarm of Sarmatia dykes, and within the WAC, the Kedougou
327 dykes dated at 1764 ± 4 Ma (Baratoux *et al.*, 2019) and the dykes of the Anti-Atlas dated at
328 1750 Ma (Youbi *et al.*, 2013).

329 At about 1520 Ma, another major thermal event having affected the WAC can be
330 inferred from the similar ages around 1519-1528 Ma recorded for the dyke swarms of
331 Essakane in the NE of Burkina Faso (1519 to 1525 Ma), of Sambarabougou in the KKI,
332 Senegal and Mali (1521 Ma) and of Käyser, Suriname, (Baratoux *et al.*, 2019). These authors
333 suggested that the Essakane-Sambarabougou-Käyser events might be a huge swarm of dykes
334 of ca. 1519-1528 Ma, associated with a LIP emplacement (Essakane LIP; Ernst and Youbi,
335 2017) within the Leo Man Shield, to the SW of the WAC and formerly adjacent to the
336 Amazonia Craton. Note that within the same crustal block, coeval LIP magmatism dated at ca
337 1500 Ma has been reported in São Francisco (South America) craton (Silveira *et al.*, 2013).

338 Our K-feldspar $^{40}\text{Ar}/^{39}\text{Ar}$ results having recorded two thermal events, together with the
339 U-Pb ages obtained for dykes in the same area, they can be tentatively interpreted as imprints
340 of successive arrival of large magmatic systems in the KKI area. However, the WAC and
341 adjacent cratons did not experience breakup at ~1750 nor ~1500 Ma. The NW of the
342 Amazonia was linked to the SW of the Baltica from at least 1.8 Ga to at least 0.8 Ga, and the
343 WAC was probably linked to the NE of the Amazonia and to the SE of the Baltica during the
344 same period (Johansson, 2009). The Amazonia and the WAC remained linked from about 2.0
345 Ga until Gondwana breakup in connection with the opening of the Southern Atlantic Ocean at
346 about 120 Ma. As breakup did not occur within the WAC in the 1800-1500 Ma interval, it is
347 tempting to propose that the two thermal events identified here in K-feldspar disturbed age
348 spectra at ~1750 and ~1500 Ma, and coeval dyke swarm emplacements, might instead only
349 correspond to several aborted attempts of continental breakup.

350

351 **6. Conclusion**

352

353 New $^{40}\text{Ar}/^{39}\text{Ar}$ ages obtained for hornblendes and biotites from the Kedougou Kenieba
354 Inlier (eastern Senegal), the western-central outcropping part of the West African Craton,
355 range between 2055 ± 26 and 2028 ± 28 Ma, in agreement with previous results from rocks
356 associated with the 2.2 - 2.0 Ga Eburnean Orogeny (Hirdes and Davis, 2002).

357 Together with the published U-Pb ages, our new $^{40}\text{Ar}/^{39}\text{Ar}$ ages show that the
358 Kedougou Kenieba Inlier was affected by two moderate thermal events reported at the scale
359 of the WAC at ~1750 and ~1500 Ma. Our well-constrained $^{40}\text{Ar}/^{39}\text{Ar}$ biotite and hornblende
360 ages argue for a relatively fast initial cooling between 5 and $20^\circ\text{C}.\text{Myr}^{-1}$ and rule out the
361 hypothesis of a significant re-heating event above 300°C after emplacement of the batholith.
362 On the other hand, disturbance of $^{40}\text{Ar}/^{39}\text{Ar}$ K-feldspars age spectra can be explained by

363 invoking two re-heating events at ~1750 and ~1500 Ma, with temperatures of about 275 and
364 225°C, respectively.

365 Mafic dyke intrusions within Kedougou Kenieba Inlier, previously reported at $1764 \pm$
366 4 Ma and 1521 ± 3 Ma from U-Pb ages (Baratoux *et al.*, 2019), could be related to these re-
367 heating events. According to their structural orientation, the first thermal event (~1750 Ma)
368 can be correlated with the dyke swarm of Tagragra of Akka in Morocco, and the second one
369 (~1500 Ma) with the dyke swarm of Käyser in Suriname (Baratoux *et al.*, 2019). As the WAC
370 remained attached to Baltica and Amazonia cratons during the 1.8-1.3 Ga interval (Johansson,
371 2009), only failed continental rifting events can be inferred from these thermal events
372 recorded in $^{40}\text{Ar}/^{39}\text{Ar}$ K-feldspars age spectra at about 1750 and 1500 Ma.

373

374

375 **Acknowledgements**

376 We are grateful to IFAN Cheikh Anta Diop from University Cheikh Anta Diop (Dakar,
377 Sénégal) for I. Sagna's visiting grants at University Paris-Sud. French Centre National de la
378 Recherche Scientifique (CNRS) and University Paris Sud supported this work. We thank
379 Renaud Merle and Jean-Paul Liégeois for their detailed reviews, which contributed to
380 significantly improve this manuscript. This is LGMT contribution number 163.

381

382

383 **References**

384

385 Abouchami, W., M. Boher, A. Michard, & Albarede F. (1990). A Major 2.1 Ga Event of
386 Mafic Magmatism in West Africa - an Early Stage of Crustal Accretion, *Journal of*
387 *Geophysical Research-Solid Earth and Planets*, 95 (B11), 17605-17629.

388 Baratoux, L., Metelka, V., Naba, S., Jessell, M. W., Grégoire, M., & Ganne, J. (2011).
389 Juvenile Paleoproterozoic crust evolution during the Eburnean orogeny (□ 2.2–2.0 Ga),
390 western Burkina Faso. *Precambrian Research*, 191(1-2), 18-45.

391 Baratoux, L., Söderlund, U., Ernst, R.E., de Roever, E., Jessell, M.W., Kamo, S., Naba, S.,
392 Perrouty, S., Metelka, V., Yatte, D., Grenholm, M., Diallo, D.P., Ndiaye, P.M., Dioh,
393 E., Cournède, C., Benoit, M., Baratoux, D., Youbi, N., Rouse, S., & Bendaoud, A.
394 (2019). New U–Pb Baddeleyite Ages of Mafic Dyke Swarms of the West African and
395 Amazonian Cratons: Implication for Their Configuration in Supercontinents Through
396 Time. In *Dyke Swarms of the World: A Modern Perspective* (pp. 263-314). Springer,
397 Singapore.

398 Bassot, J.P. (1966). Etude géologique du Sénégal oriental et de ses confins Guinéo-Maliens.
399 Mémoires Bureau Recherches Géologiques, 40, 332pp.

400 Bassot, J.P. (1987). Le complexe volcano–plutonique calco–alcalin de la rivière Daléma (Est
401 du Sénégal): discussion de sa signification géodynamique dans le cadre de l’orogène
402 éburnéenne (Protérozoïque inférieur). *Journal of African Earth Sciences*, 6, n°. 4, 505–
403 519.

404 Begg, G.C., W.L. Griffin, L.M. Natapov, S.Y. O'Reilly, S.P. Grand, C.J. O'Neill, J.M.A.
405 Hronsky, Y.P. Djomani, C.J. Swain, T. Deen, & Bowden P. (2009). The lithospheric
406 architecture of Africa: Seismic tomography, mantle petrology, and tectonic evolution,
407 *Geosphere*, 5 (1), 23-50.

408 Cahen, L., Snelling, N.J., Delhail, J., & Vail, J.R. (1984). The Geochronology and Evolution

409 of Africa. Clarendon Press, London.

410 Coulié, E., Quidelleur, X., Lefèvre, J.C., & Gillot, P.Y. (2004). Exploring the multicollection
411 approach for the $^{40}\text{Ar}/^{39}\text{Ar}$ dating technique. *Geochemistry Geophysics Geosystems* 5.

412 Dia, A. (1988). Caractères et signification des complexes magmatiques et métamorphiques du
413 secteur de Sandikounda–Laminia (Nord de la Boutonnière de Kédougou; Est du
414 Sénégal): un modèle géodynamique du Birrimien de l’Afrique de l’Ouest. Unpubl. Ph.
415 D. thesis, 350pp. Université de Dakar, Sénégal.

416 Dia, A., W.R. VanSchmus, & A. Kroner (1997). Isotopic constraints on the age and formation
417 of a Palaeoproterozoic volcanic arc complex in the Kedougou Inlier, eastern Senegal,
418 West Africa, *Journal of African Earth Sciences*, 24 (3), 197-213.

419 Dioh, E., D. Beziat, P. Debat, M. Gregoire, & P.M. Ngom (2006). Diversity of the
420 Palaeoproterozoic granitoids of the Kedougou inlier (eastern Senegal): Petrographical
421 and geochemical constraints, *Journal of African Earth Sciences*, 44 (3), 351-371.

422 Ernst R.E. (2014) *Large Igneous Provinces*. Cambridge University Press, p 653.

423 Ernst, R. E., & Youbi, N. (2017). How Large Igneous Provinces affect global climate,
424 sometimes cause mass extinctions, and represent natural markers in the geological
425 record. *Palaeogeography, palaeoclimatology, palaeoecology*, 478, 30-52.

426 Feybesse, J. L., Billa, M., Guerrot, C., Duguey, E., Lescuyer, J. L., Milesi, J. P., & Bouchot,
427 V. (2006). The paleoproterozoic Ghanaian province: Geodynamic model and ore
428 controls, including regional stress modeling. *Precambrian Research*, 149(3-4), 149-196.

429 Fleck, R. J., Sutter, J. F., & Elliot, D. H. (1977). Interpretation of discordant $^{40}\text{Ar}/^{39}\text{Ar}$ age-
430 spectra of Mesozoic tholeiites from Antarctica. *Geochimica et Cosmochimica*
431 *Acta*, 41(1), 15-32.

432 Goujou, J.-C., Buscail, F., Theveniaut, H., Dioh, E., Delor, C., Bleinok, Diallo, D.P., Ndiaye,
433 P.M., Le Metour, J., Fullgraf, T., Caby, R., Couëffe, R., Martelet, G., Sergeev, S.,

434 Villeneuve, M., & Wemmer, K. (2010). Notice explicative Carte géologique à 1/200
435 000 du Sénégal, *feuille Kossanto-Dalafi Est. Ministère des Mines, de l'Industrie, de*
436 *l'Agro-industrie et des PME, Direction des Mines et de la Géologie, Dakar.*

437 Gueye, M., S. Siegesmund, K. Wemmer, S. Pawlig, A. Drobe, N. Nolte, & P. Layer (2007).
438 New evidences for an early Birimian evolution in the West African Craton: An example
439 from the Kedougou-Kenieba inlier, southeast Senegal, *South African Journal of*
440 *Geology*, 110 (4), 511-534.

441 Harrison, T.M., & I. McDougall (1980). Investigations of an intrusive contact, northwest
442 Nelson, New Zealand—II. Diffusion of radiogenic and excess ^{40}Ar in hornblende
443 revealed by $^{40}\text{Ar}/^{39}\text{Ar}$ age spectrum analysis, *Geochimica Et Cosmochimica Acta*, 44,
444 2005-2020.

445 Hartmann, L. A. (2002). The Mesoproterozoic supercontinent Atlantica in the Brazilian
446 shield-review of geological and U-Pb zircon and Sm-Nd isotopic evidence. *Gondwana*
447 *Research*, 5(1), 157-163.

448 Hastie, W., Watkeys, M., & Aubourg, C. (2014). Magma flow in dyke swarms of the Karoo
449 LIP: Implications for the mantle plume hypothesis. *Gondwana Research*, 25, 736-755.

450 Hirdes, W., & Davis, D. W. (2002). U–Pb geochronology of paleoproterozoic rocks in the
451 southern part of the Kedougou-Kenieba Inlier, Senegal, West Africa: evidence for
452 diachronous accretionary development of the Eburnean province. *Precambrian*
453 *Research*, 118(1-2), 83-99.

454 Hodges, K.V. (1991). Pressure–temperature–time paths. *Annual Review of Earth and*
455 *Planetary Sciences* 19, 207–236.

456 Jessell, M.W., Santoul, J., Baratoux, L. Youbi, N., Ernst, R.E., Metelka, V., Miller, J., &
457 Perrouty, S. (2015). An updated map of West African mafic dykes. *Journal of African*
458 *Earth Sciences* 112(B): 440–450.

- 459 Johansson, Å. (2009). Baltica, Amazonia and the SAMBA connection—1000 million years of
460 neighbourhood during the Proterozoic? *Precambrian Research*, 175(1-4), 221-234.
- 461 Johansson, Å. (2014). From Rodinia to Gondwana with the ‘SAMBA’ model—a distant view
462 from Baltica towards Amazonia and beyond. *Precambrian Research*, 244, 226-235.
- 463 Jourdan, F., Bertrand, H., Schärer, U., Blichert-Toft, J., Féraud, G. and Kampunzu, A.B.
464 (2007). Major and trace element and Sr, Nd, Hf, and Pb isotope compositions of the
465 Karoo Large Igneous Province, Botswana-Zimbabwe : Lithosphere vs Mantle plume
466 Contribution. *Journal of Petrology*, 48(6), 1043-1077.
- 467 Kone, J., Baratoux, L., Maneiro, K., Baxter, E., Vanderhaeghe, O., Duchène, S.,
468 Ndiaye, P.M., Pitra, P., Dufrechou, G., & Bruguier, O. (2018) *Goldschmidt*
469 *Abstracts*, 2018, 1328.
- 470 Kroonenberg, S. B., De Roever, E. W. F., Fraga, L. M., Reis, N. J., Faraco, T., Lafon, J. M.,
471 Cordani, U., & Wong, T.E. (2016). Paleoproterozoic evolution of the Guiana Shield in
472 Suriname: A revised model. *Netherlands Journal of Geosciences*, 95(4), 491-522.
- 473 Kuiper, K.F., Deino, A., Hilgen, F.J., Krijgsman, W., Renne, P.R., & Wijbrans, J.R. (2008).
474 Synchronizing Rock Clocks of Earth History. *Science* 320, 500–504.
- 475 Lee, J.K.W., Williams, I.S., & Ellis, D.J. (1997). Pb, U and Th diffusion in natural zircon.
476 *Nature* 390, 159–162.
- 477 Li, Z. X., Li, X. H., Kinny, P. D., & Wang, J. (1999). The breakup of Rodinia: did it start with
478 a mantle plume beneath South China?. *Earth and Planetary Science Letters*, 173(3),
479 171-181.
- 480 Lovera, O.M., Richter, F.M., & Harrison, T.M. (1989). $^{40}\text{Ar}/^{39}\text{Ar}$ geothermometry for slowly
481 cooled samples having a distribution of diffusion domain sizes. *Journal of Geophysical*
482 *Research*, 94, 17917-17935.
- 483 Lovera, O.M. (1992). Computer programs to model $^{40}\text{Ar}/^{39}\text{Ar}$ diffusion data from multi-

484 domain samples. *Computers and Geosciences*, 18, 789-813.

485 Lovera, O.M., Grove, M., Harrison, T.M., & Mahon, K.I. (1997). Systematic analysis of K
486 feldspar $^{40}\text{Ar}/^{39}\text{Ar}$ step-heating experiments I: Significance of activation energy
487 determinations. *Geochimica Cosmochimica Acta*, 61, 3171-3192

488 McDougall, I., & T.M. Harrison (1999). *Geochronology and thermochronology by the*
489 *$^{40}\text{Ar}/^{39}\text{Ar}$ method*, 269 pp., Oxford Univ. Press, New York.

490 Marzoli, A., Renne, P. R., Piccirillo, E. M., Ernesto, M., Bellieni, G., & De Min, A. (1999).
491 Extensive 200-million-year-old continental flood basalts of the Central Atlantic
492 Magmatic Province. *Science*, 284(5414), 616-618.

493 Maurel, O., Respaut, J. P., Monié, P., Arnaud, N., & Brunel, M. (2004). U/ Pb emplacement
494 and $^{40}\text{Ar}/^{39}\text{Ar}$ cooling ages of the eastern Mont-Louis granite massif (Eastern Pyrenees,
495 France). *Comptes Rendus Geoscience*, 336(12), 1091-1098.

496 Merle, R., Marzoli, A., Bertrand, H., Reisberg, L., Verati, C., Zimmermann, C., Chiaradia,
497 M., Bellieni, G., & Ernesto, M. (2011). $^{40}\text{Ar}/^{39}\text{Ar}$ ages and Sr–Nd–Pb–Os geochemistry
498 of CAMP tholeiites from Western Maranhão basin (NE Brazil). *Lithos*, 122(3-4), 137-
499 151.

500 Merle, R., Marzoli, A., Reisberg, L., Bertrand, H., Nemchin, A., Chiaradia, M., Callegaro,
501 S., Jourdan, F., Bellieni, G., Kontak, D., Puffer, J., & McHone, J.G. (2014). Sr, Nd, Pb
502 and Os isotope systematics of CAMP tholeiites from Eastern North America (ENA):
503 evidence of a subduction-enriched mantle source. *Journal of Petrology*, 55(1), 133-180.

504 Ndiaye, P., Robineau, B., & Moreau, C. (1989). Deformation and metamorphism of Birrimian
505 formations, in relation to the emplacement of the Eburnean Saraya granite (eastern
506 Senegal). *Bulletin De La Société Géologique De France*, 5(3), 619-625.

507 Neves, S. P., Bruguier, O., Vauchez, A., Bosch, D., Da Silva, J. M. R., & Mariano, G. (2006).
508 Timing of crust formation, deposition of supracrustal sequences, and Transamazonian

509 and Brasiliano metamorphism in the East Pernambuco belt (Borborema Province, NE
510 Brazil): implications for western Gondwana assembly. *Precambrian Research*, 149(3-
511 4), 197-216.

512 Nomade, S., Féraud, G., Chen, Y., & Pouclet, A. (2002). Thermal and tectonic evolution of
513 the paleoproterozoic Transamazonian orogen as deduced from $^{40}\text{Ar}/^{39}\text{Ar}$ and AMS
514 along the Oyapok river (French Guyana). *Precambrian Research*, 114(1-2), 35-53.

515 Nomade, S., Knight, K. B., Beutel, E., Renne, P. R., Verati, C., Féraud, G., Marzoli, A.,
516 Youbi, N., & Bertrand, H. (2007). Chronology of the Central Atlantic Magmatic
517 Province: implications for the Central Atlantic rifting processes and the Triassic–
518 Jurassic biotic crisis. *Palaeogeography, Palaeoclimatology, Palaeoecology*, 244(1-4),
519 326-344.

520 Park, J. K., Buchan, K. L., & Harlan, S. S. (1995). A proposed giant radiating dyke swarm
521 fragmented by the separation of Laurentia and Australia based on paleomagnetism of
522 ca. 780 Ma mafic intrusions in western North America. *Earth and Planetary Science
523 Letters*, 132(1-4), 129-139.

524 Perrouty, S., Aillères, L., Jessell, M. W., Baratoux, L., Bourassa, Y., & Crawford, B. (2012).
525 Revised Eburnean geodynamic evolution of the gold-rich southern Ashanti Belt, Ghana,
526 with new field and geophysical evidence of pre-Tarkwaian deformations. *Precambrian
527 Research*, 204, 12-39.

528 Phillips, D., Matchan, E. L., Honda, M., & Kuiper, K. F. (2017). Astronomical calibration of
529 $^{40}\text{Ar}/^{39}\text{Ar}$ reference minerals using high-precision, multi-collector (ARGUSVI) mass
530 spectrometry. *Geochimica et Cosmochimica Acta*, 196, 351-369.

531 Quidelleur, X., Grove, M., Lovera, O. M., Harrison, T. M., Yin, A., & Ryerson, F. J. (1997).
532 Thermal evolution and slip history of the Renbu Zedong Thrust, southeastern
533 Tibet. *Journal of Geophysical Research: Solid Earth*, 102(B2), 2659-2679.

- 534 Renne, P.R., Mundil, R., Balco, G., Min, K., & Ludwig, K.R. (2010). Joint determination of
535 ^{40}K decay constants and $^{40}\text{Ar}/^{40}\text{K}$ for the Fish Canyon sanidine standard, and improved
536 accuracy for $^{40}\text{Ar}/^{39}\text{Ar}$ geochronology. *Geochimica et Cosmochimica Acta* 74, 5349–
537 5367.
- 538 Ricci, J., Quidelleur, X., Pavlov, V., Orlov, S., Shatsillo, A., & Courtillot, V. (2013). New
539 $^{40}\text{Ar}/^{39}\text{Ar}$ and K-Ar ages of the Viluy traps (Eastern Siberia): Further evidence for a
540 relationship with the Frasnian – Famennian mass extinction. *Palaeogeography,*
541 *Palaeoclimatology, Palaeoecology* 386, 531–540.
- 542 Sagna, I., Quidelleur, X., Ndiaye, Fr., Gillot, P.-Y., Lefèvre, J.-C., & Dioh, E. (2017). K–Ar
543 mineral ages and thermal history of magmatic and metamorphic Palaeoproterozoic units
544 from the northern part of Kedougou Kenieba Inlier, West African Craton (Eastern
545 Senegal), *Geological Journal* 52, 207–216.
- 546 Schofield, D. I., Horstwood, M. S. A., Pitfield, P. E. J., Gillespie, M., Darbyshire, F.,
547 O’Connor, E. A., & Abdouloye, T. B. (2012). U–Pb dating and Sm–Nd isotopic analysis
548 of granitic rocks from the Tiris Complex: New constraints on key events in the evolution
549 of the Reguibat Shield, Mauritania. *Precambrian Research*, 204, 1-11.
- 550 Silveira, E. M., Söderlund, U., Oliveira, E. P., Ernst, R. E., & Leal, A. M. (2013). First precise
551 U–Pb baddeleyite ages of 1500 Ma mafic dykes from the São Francisco Craton, Brazil,
552 and tectonic implications. *Lithos*, 174, 144-156.
- 553 Steiger, R.H., & E. Jäger (1977). Subcommission on Geochronology: convention on the use
554 of decay constants in Geo and Cosmochronology, *Earth Planet. Sci. Lett.*, 36, 359-362.
- 555 Tait, J., Straathof, G., Söderlund, U. Ernst, R. E.; Key, R.; Jowitt, S. M.; Lo, K.; Dahmada, M.
556 E. M., & N'Diaye, O. (2013) The Ahmeyim Great Dyke of Mauritania: a newly dated
557 Archaean intrusion. *Lithos* 174:323–332.

558 Theveniaut, H., Ndiaye, P.M., Buscail, F., Couëffé, R., Delor, C., Fullgraf, T. & Goujou, J.C.
559 (2010). Notice explicative de la carte géologique à 1/500 000 du Sénégal oriental.
560 *Ministère des Mines, de l'Industrie, de l'Agro-industrie et des PME, Direction des*
561 *Mines et de la Géologie, Dakar, 119p.*

562 Thiéblemont, D., Goujou, J. C., Egal, E., Cocherie, A., Delor, C., Lafon, J. M., & Fanning, C.
563 M. (2004). Archean evolution of the Leo Rise and its Eburnean reworking. *Journal of*
564 *African Earth Sciences, 39(3-5), 97-104.*

565 Tshibubudze, A., Hein, K. A. A., Peters, L. F. H., Woolfe, A. J., & McCuaig, T. C. (2013).
566 Oldest U-Pb crystallisation age for the West African Craton From the Oudalan-Gorouol
567 Belt of Burkina Faso. *South African Journal of Geology, 116(1), 169-181.*

568 Wane, O., Liégeois, J. P., Thébaud, N., Miller, J., Metelka, V., & Jessell, M. (2018). The
569 onset of the Eburnean collision with the Kenema-Man craton evidenced by plutonic and
570 volcanosedimentary rock record of the Masssigui region, southern Mali. *Precambrian*
571 *Research, 305, 444-478.*

572 Wartho, J.-A., Dodson, M. H., Rex, D. C., & Guise, P. G. (1991). Mechanisms of Ar release
573 from Himalayan metamorphic hornblende. *Am. Mineral. 76, 1446-1448.*

574 Westerhold T., Röhl U., & Laskar J. (2012) Timescale contro-versy: accurate orbital
575 calibration of the early Paleogene. *Geochem. Geophys. Geosyst. 13, Q06015.*

576 Wingate, M. T., & Giddings, J. W. (2000). Age and palaeomagnetism of the Mundine Well
577 dyke swarm, Western Australia: implications for an Australia–Laurentia connection at
578 755 Ma. *Precambrian Research, 100(1), 335-357.*

579 Youbi, N., Kouyaté, D., Söderlund, U., Ernst, R.E., Soullaimani, A., Hafid, A., Ikenne, M., El
580 Bahat, A., Bertrand, H., Chaham, K.R., Ben Abbou, M., Mortaji, A., El Ghorfi, M.,
581 Zouhair, M., & El Janati, M. (2013). The 1750 Ma Magmatic Event of the West African
582 Craton (Anti-Atlas, Morocco), *Precambrian Research 236, 106-123.*

583 Zhao, G., Cawood, P. A., Wilde, S. A., & Sun, M. (2002). Review of global 2.1–1.8 Ga
584 orogens: implications for a pre-Rodinia supercontinent. *Earth-Science Reviews*, 59,
585 125-162.
586

587 **Figure captions**

588

589

590 **Figure 1**

591 a) Geological sketch map of principal areas of the West African Craton. The thick frame
592 shows the location of Figure 1b

593 b) Geological map of the studied area within the Kedougou Kenieba Inlier and location of
594 analyzed samples (modified after Dioh *et al.*, 2006; dyke location after Jessell *et al.*, 2015).

595

596 **Figure 2**

597 a) $^{40}\text{Ar}/^{39}\text{Ar}$ apparent age spectra determined from Ar isotope data for hornblende and biotite
598 samples. The plateau age is calculated for steps shown by the arrow. Analytical uncertainty,
599 and total (i.e. including J-factor error) uncertainty (in parentheses) are given at the two-sigma
600 level.

601 b) Same as a) for K-feldspars samples.

602

603 **Figure 3**

604 Thermal history of the studied area based on K-feldspar $^{40}\text{Ar}/^{39}\text{Ar}$ ages (shown as inserts), and
605 hornblende and biotite $^{40}\text{Ar}/^{39}\text{Ar}$ ages (dashed square). The two thermal events inferred are
606 shown as 1 and 2. The blue line in each insert shows the modelled age spectra based on this
607 thermal history. The same activation energy value of 42 kcal.mol⁻¹, the lowermost value
608 obtained from monotonic cooling modeling, was used for all K-feldspars. Note that it is close
609 to the average value of 46 kcal.mol⁻¹ derived from a large K-feldspars dataset (Lovera *et al.*,
610 1997).

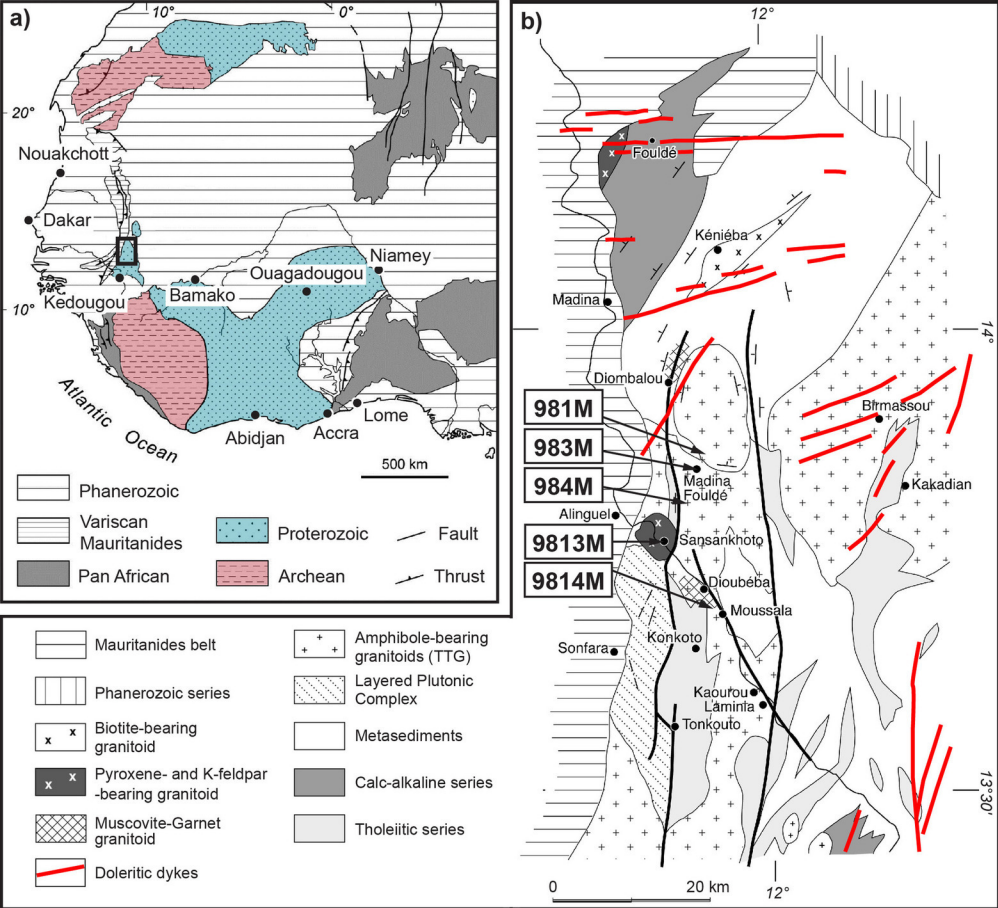


Figure 1 (Sagna et al.)

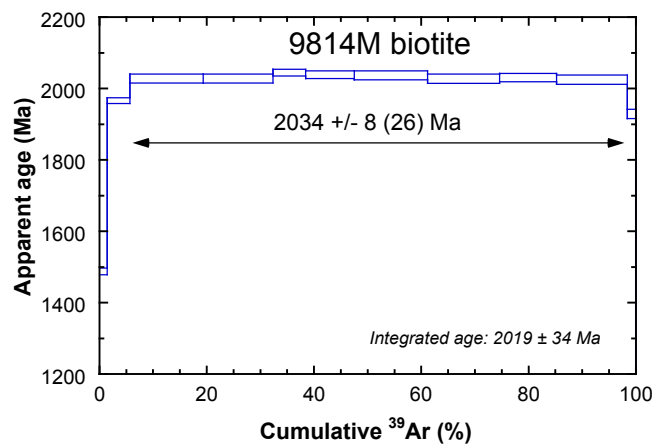
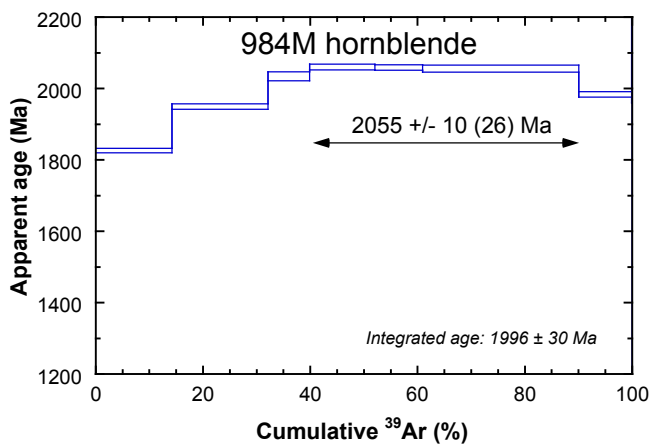
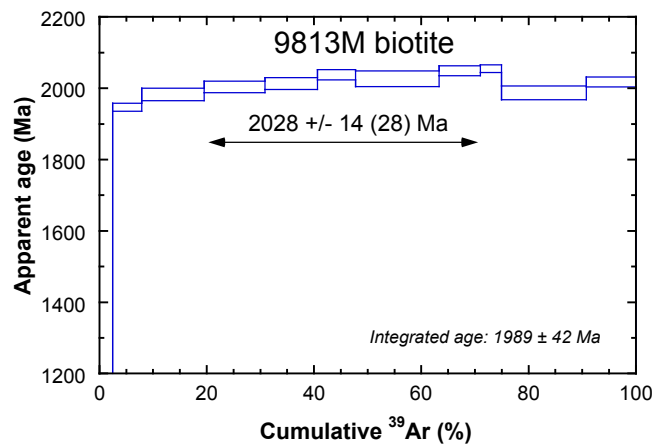
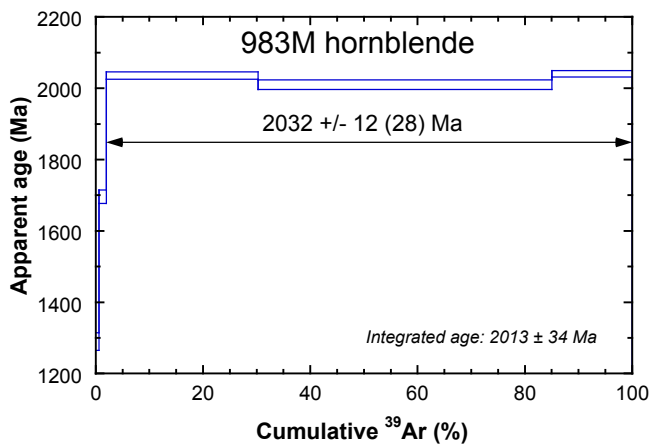
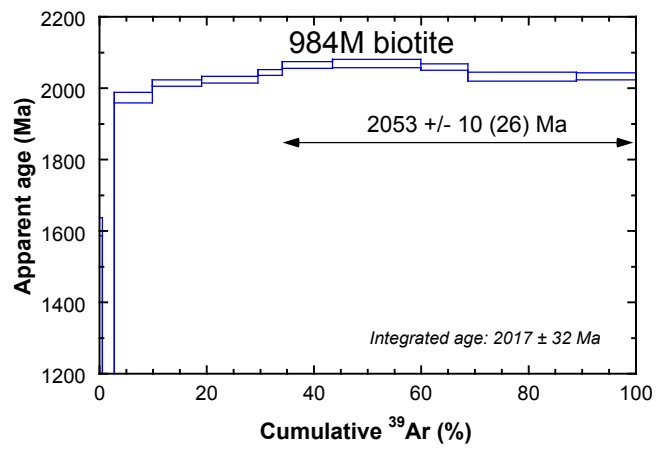
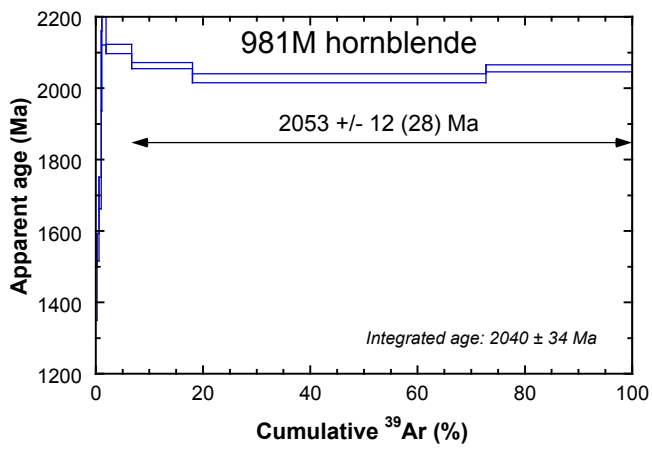


Figure 2a (Sagna et al.)

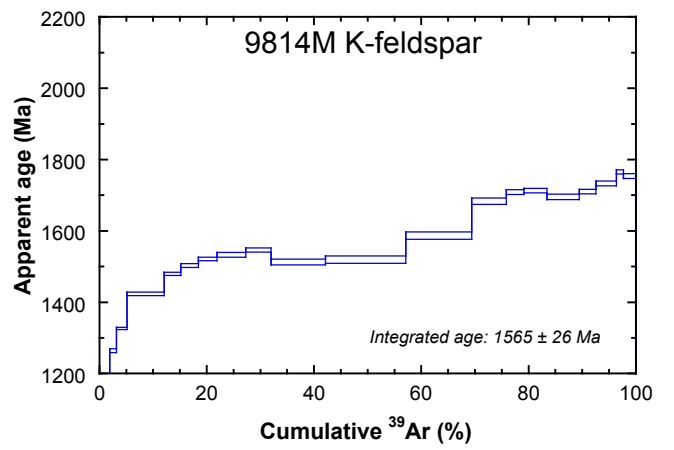
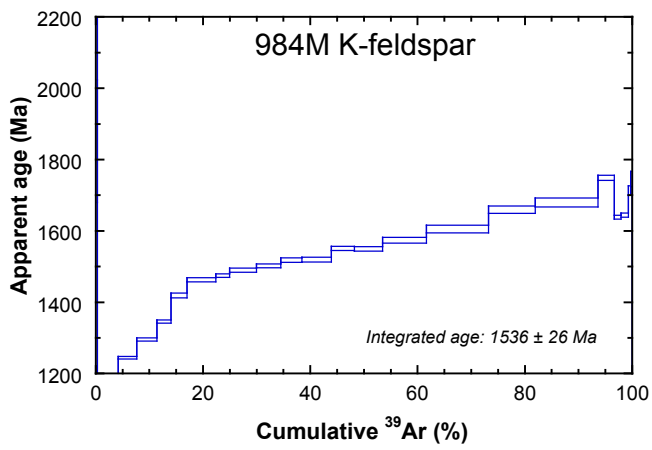
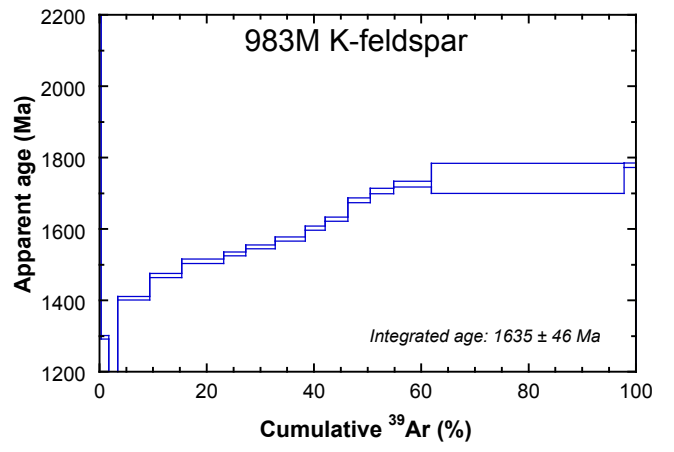
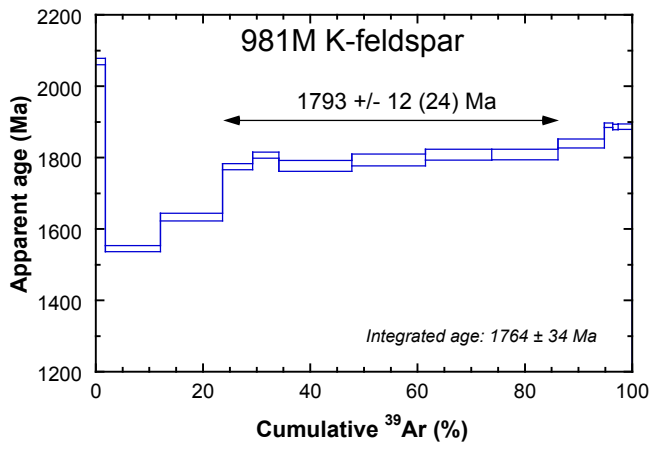


Figure 2b (Sagna et al.)

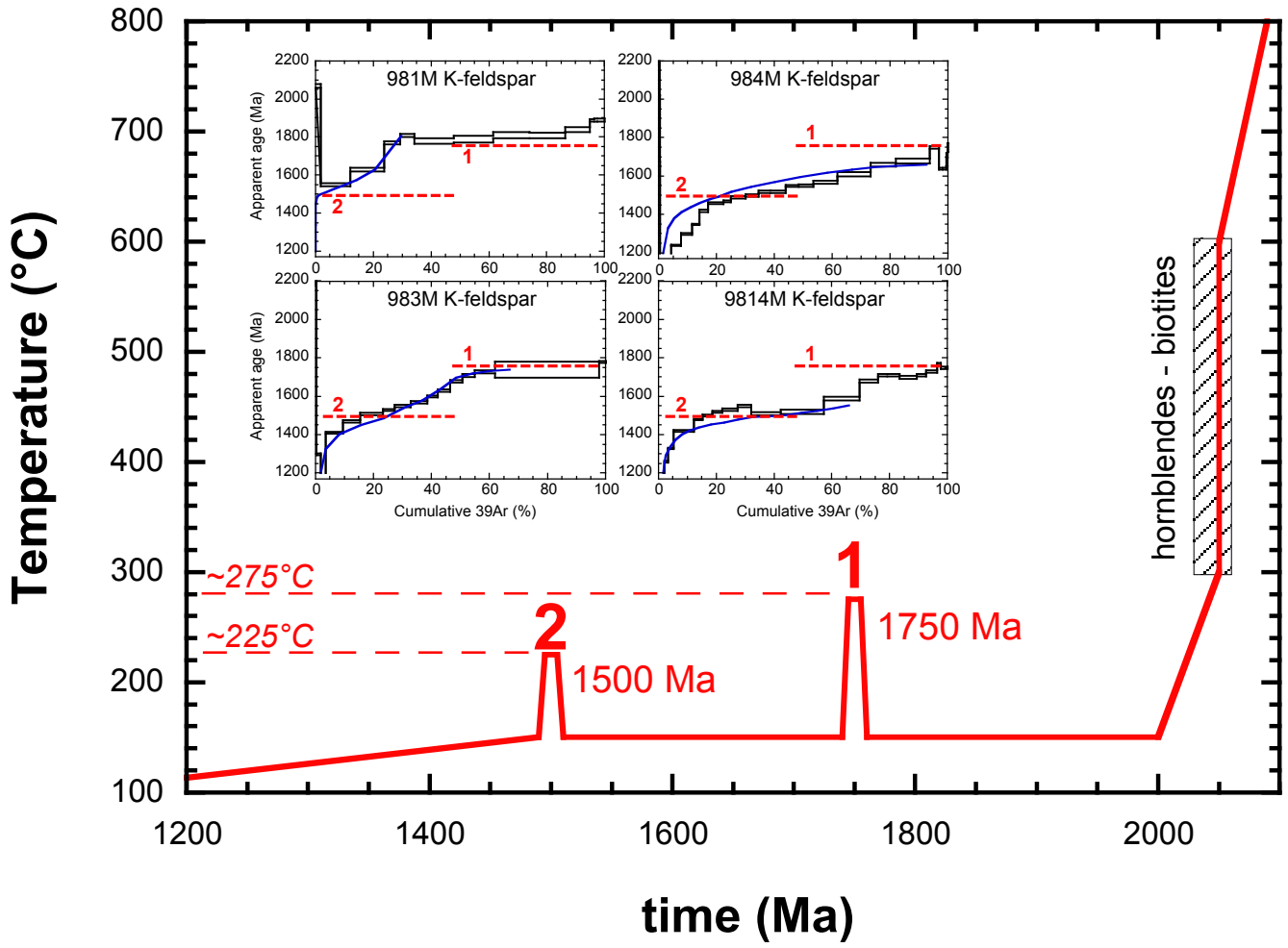


Figure 3 (Sagna et al.)